

# Factors affecting the spatial pattern of bedrock groundwater recharge at the hillslope scale

Willemijn M. Appels,<sup>1\*</sup> Chris B. Graham,<sup>2</sup> Jim E. Freer<sup>3</sup> and Jeffrey J. McDonnell<sup>1,4,5</sup>

<sup>1</sup> Global Institute for Water Security, University of Saskatchewan, Saskatoon, Canada

<sup>2</sup> Hetchy Hetchy Water and Power, Moccasin, CA, USA

<sup>3</sup> School of Geographical Sciences, University of Bristol, Bristol, UK

<sup>4</sup> School of Geosciences, University of Aberdeen, Aberdeen, UK

<sup>5</sup> Department of Forest Engineering, Resources and Management, Oregon State University, Corvallis, OR, USA

## Abstract:

The spatial patterns of groundwater recharge on hillslopes with a thin soil mantle overlying bedrock are poorly known. Complex interactions between vertical percolation of water through the soil, permeability contrasts between soil and bedrock and lateral redistribution of water result in large spatial variability of water moving into the bedrock. Here, we combine new measurements of saturated hydraulic conductivity of soil mantle and bedrock of the well-studied Panola Mountain experimental hillslope with previously collected (sub)surface topography and soil depth data to quantify the factors affecting the spatial pattern of bedrock groundwater recharge.

We use geostatistical characteristics of the measured permeability to generate spatial fields of saturated hydraulic conductivity for the entire hillslope. We perform simulations with a new conceptual model with these random fields and evaluate the resulting spatial distribution of groundwater recharge during individual rainstorms and series of rainfall events. Our simulations show that unsaturated drainage from soil into bedrock is the prevailing recharge mechanism and accounts for 60% of annual groundwater recharge. Therefore, soil depth is a major control on the groundwater recharge pattern through available storage capacity and controlling the size of vertical flux. The other 40% of recharge occurs during storms that feature transient saturation at the soil-bedrock interface. Under these conditions, locations that can sustain increased subsurface saturation because of their topographical characteristics or those with high bedrock permeability will act as hotspots of groundwater recharge when they receive lateral flow. Copyright © 2015 John Wiley & Sons, Ltd.

KEY WORDS groundwater recharge; spatial patterns; conceptual modelling

Received 31 August 2014; Accepted 3 March 2015

## INTRODUCTION

The hierarchy of controls on patterns of groundwater recharge (GWR) at varying spatial scales is poorly understood (Scanlon *et al.*, 2002). At the regional and watershed scale, where GWR is the renewable resource of large aquifers, recent research has demonstrated the vulnerability of GWR because of land use and climate change (Barron *et al.*, 2012; Flint *et al.*, 2012; Mair *et al.*, 2013). At smaller spatial scales of 1–10 m<sup>2</sup>, lysimeter and tracer studies have shown large temporal variation in such point-scale recharge fluxes under different climate regimes (Allison *et al.*, 1994; Pangle *et al.*, 2014).

Few investigations have yet examined hillslope-scale controls on the spatio-temporal variability of GWR. This

is problematic because hillslopes are the fundamental hydrological unit (Troch *et al.*, 2013) and the scale at which flow accumulation occurs in the landscape. Therefore, a key challenge in GWR research is the prediction and assessment of its variability at the hillslope scale (Allison *et al.*, 1994; De Vries and Simmers, 2002). Although spatial variability of GWR at hillslope scale may not be critical for water resource management (Flint *et al.*, 2012), it may have profound implications for solute and contaminant transport. Zones of focused recharge can allow contaminants to move quickly from the unsaturated zone to underlying aquifers and streams (Scanlon *et al.*, 2002). Here, we define hillslope GWR as all water that is transferred from the soil into the bedrock, where it is no longer available for root water uptake.

At the hillslope scale, such recharge may feed aquifers through deep percolation and fast flow through fractures that may contribute to catchment streamflow farther down valley (Torres *et al.*, 1998; Montgomery and Dietrich, 2002;

\*Correspondence to: Willemijn M. Appels, Global Institute for Water Security, University of Saskatchewan, Saskatoon, Canada.  
E-mail: willemijn.appels@usask.ca

Gleeson *et al.*, 2009; Graham *et al.*, 2010; Gabrielli *et al.*, 2012).

At the hillslope scale, the partitioning of infiltrating water in lateral flow (often during events) and continued vertical flow into underlying glacial drift, saprolite or weathered rock exhibits large spatio-temporal variability. Heppner *et al.* (2007) estimated yearly GWR of 21–52% of annual rainfall under a grass lysimeter during 5 years of natural rainfall conditions. Experiments on small hillslopes have estimated event-scale GWR as a percentage of storm precipitation of 34–41% (Ontario, Canada; Buttle and McDonald, 2002), 41% (Oregon, USA; Graham *et al.*, 2010), 35–55% (Japan; Kosugi *et al.*, 2006) and 94% (Georgia, USA; Tromp-van Meerveld *et al.*, 2007), while runoff ratios (i.e. the lateral flow percentage) on these hillslopes have been estimated to be respectively 30–43% (Peters *et al.*, 1995), 13% (Gabrielli *et al.*, 2012), 3.5–7.4% (Kosugi *et al.*, 2006) and 5% (Tromp-van Meerveld and McDonnell, 2006a).

Depending on the nature and variability of the soil-bedrock interface (SBI), the volume of water that moves vertically past the SBI can be equal to or larger than the volume of water that is routed laterally downslope along that interface. These relative values depend mainly on bedrock permeability, soil depth and slope angle (Asano *et al.*, 2002; Ebel and Loague, 2008; Hopp and McDonnell, 2009). Spatial variability of bedrock permeability can cause variations in return flow from bedrock into soil (Wilson and Dietrich, 1987; Shand *et al.*, 2007). Hillslopes rarely experience a uniformly rising and falling perched groundwater table at the SBI (Salve *et al.*, 2012). The filling, leakage and lateral spilling of hillslope-scale patches of transient saturation at the SBI (Tromp van Meerveld and McDonnell, 2006b) are now seen as a common behaviour across many environments (Bachmair and Weiler, 2011; McDonnell, 2013). However, the GWR consequences of this behaviour have not yet been examined.

Here, we present new measurements and new model results from the well-described Panola experimental hillslope (see Tromp-van Meerveld and McDonnell (2009) for a site review) to examine the hierarchy of factors affecting the spatial pattern of bedrock GWR (at the hillslope scale). Considering the known bedrock topography and bedrock permeability at this hillslope, we hypothesize that saturation at the SBI is a driver of increased bedrock GWR. We further hypothesize that rainfall dynamics are an important on/off switch for GWR patterns. We developed a new model (building upon Appels *et al.* (2011)) to examine a number of specific questions:

- How do spatial patterns of soil- and bedrock hydraulic conductivity (derived from new point-scale measurements) influence hillslope-scale transient soil saturation and resulting bedrock GWR?
- What is the sequence of controls on the spatial pattern of GWR?
- How do within-storm and between-storm rainfall conditions influence this sequencing and ultimate process hierarchy?

## STUDY SITE

The study hillslope is part of the Panola Mountain Research Watershed (PMRW), located in the Georgia Piedmont, southeast of Atlanta (GA, USA). In 1995, a 29 × 51 m hillslope was instrumented with 135 crest-stage gauges, 29 recording wells and a 20-m-wide-trench at the downhill boundary, excavated down to competent bedrock. Detailed site and instrumentation descriptions can be found elsewhere (Freer *et al.*, 2002; Tromp-van Meerveld and McDonnell, 2006a, 2006b, 2007, 2009). Here, we only describe the soil and bedrock characteristics that are relevant for the current modelling study.

The PMRW is underlain by Panola Granite bedrock, a 300- to 360-Ma old biotite-oligoclase-quartz-microcline granite formation. The primary conductivity of the granite matrix is estimated to be  $7 \times 10^{-6} \text{ m year}^{-1}$ , with a secondary regolith conductivity of  $1 \times 10^{-3} \text{ m year}^{-1}$  (White *et al.*, 2001). The effective hydraulic conductivity of the weathered granite was found to be in the range of  $8.8 \times 10^{-8}$  to  $5.1 \times 10^{-6} \text{ m s}^{-1}$  in falling head experiments (White *et al.*, 2002) and  $1.6 \times 10^{-6} \text{ m s}^{-1}$  in an area-average sprinkling experiment (Tromp-van Meerveld *et al.*, 2007).

Throughout the watershed, the top 2–4 m of the bedrock is weathered to porous soft disintegrated granite (saprolite) that has retained the original granodiorite texture (White *et al.*, 2001). Tromp-van Meerveld *et al.* (2007) did not find saprolite at the monitored hillslope site, except at the deepest soil section, 20–22 m upslope from the trench face (Figure 1).

The soil depth ranges from 0.0 to 1.8 m (average 0.63 m) and consists of hillslope sediments and colluvium from upslope erosion (Freer *et al.*, 1997; White *et al.*, 2001; Tromp-van Meerveld *et al.*, 2007). The coarse sandy loam does not have pronounced layering or discernible structure except for a 0.15-m-thick organic horizon (Tromp-van Meerveld and McDonnell, 2006a). A large part of subsurface flow captured at the hillslope trench at the slope base takes place in macropores and soil pipes (Freer *et al.*, 2002; Tromp-van Meerveld and McDonnell, 2006b).

Average seasonal hillslope runoff coefficients for fall, winter, spring and summer periods are 6%, 10%, 1% and <1%, respectively, resulting in a yearly average hillslope runoff coefficient of 5% (Tromp-van Meerveld and McDonnell, 2006a). Accounting for evapotranspiration

## SPATIAL PATTERNS OF BEDROCK GROUNDWATER RECHARGE

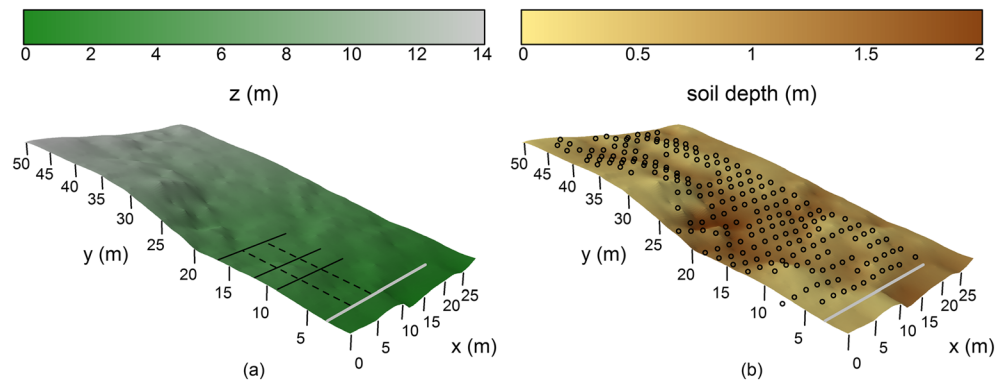


Figure 1. (a) Bedrock topography of the Panola hillslope, interpolated to a  $0.25 \times 0.25$  m grid. The grey line indicates the position of the trench. The black solid lines indicate the position of the sprinkling lines, and the dashed lines indicate the projected trench sections for which bedrock losses could be determined. (b) Soil depth distribution of the Panola hillslope, interpolated to a  $0.25 \times 0.25$  m grid. The circles indicate the location of the wells. The grey line indicates the position of the trench. The actual values of hydraulic conductivity are shown in Figure 2 and Table III

by the oak-hickory forest, GWR losses to the bedrock are greater than 20% of precipitation during large storm events, reaching 90–95% during artificial sprinkling events (Tromp-van Meerveld *et al.*, 2007). Overland flow does not occur on the hillslope, except on the small section of exposed bedrock.

## METHODS

*Measurements of saturated hydraulic conductivity of soil and bedrock*

We measured vertical soil hydraulic conductivity in two transects of 240-m and 285-m length with a Guelph permeameter at a maximum of four depths (0.19, 0.32, 0.46 and 0.75 m). The transects were located perpendicular to the main stream channel downhill of the study site in a ridge and hollow on the hillslope. Each transect featured four measurement sites.

Lateral saturated hydraulic conductivity of the soil immediately above the bedrock was measured through falling head well tests in 135 wells, forming a very approximate  $2 \times 2$  m grid (Figure 1b). The wells were composed of 1.9 cm PVC pipes, augered to bedrock and screened over the bottom 0.10 m. A 1 l bottle was fixed to the top of the well and the time needed to drain the 1 l bottle was recorded. This experiment was repeated until steady state conditions were reached. Some wells were positioned in areas with either soil pipes or cracks and water could not be supplied at a rate high enough to quantify drawdown. No lateral saturated conductivity could be calculated from these wells.

The lateral conductivity  $K_L$  was calculated with the Bouwer and Rice (1976) method for slug tests:

$$K_L = \frac{r_c^2 \ln(R_e/r_w)}{2L_e} \frac{1}{t} \ln\left(\frac{y_0}{y_t}\right) \quad (1)$$

where  $r_c$  is the radius of the well casing (m),  $r_w$  is the radius of the well including the gravel envelope (m),  $R_e$  is the radial distance over which the head is dissipated (m),  $L_e$  is the length of the screen (m),  $t$  is time (s),  $y_0$  is the drawdown at  $t=0$  (m) and  $y_t$  is the drawdown at time  $t=t$  (m).

The estimation of  $\ln(R_e/r_w)$  for a fully penetrating well is given by the following:

$$\ln(R_e/r_w) = \left[ \frac{1.1}{\ln(L_w/r_w)} + \frac{C}{L_e/r_w} \right]^{-1} \quad (2)$$

where  $L_w$  is the length of the well in the aquifer (m) and  $C$  is a dimensionless coefficient that is a function of  $L_e/r_w$  (–). The calculated  $K_L$  combines both effects of conductivity and the local bedrock gradient. We analysed the results to see if the local gradient systematically affected the measured  $K$  value. It was assumed that the soil permeability was greater than that of the bedrock, and the majority of flow would be lateral rather than vertical, leading to estimates of lateral rather than vertical hydraulic conductivity.

The bedrock hydraulic conductivity was measured during three sprinkling experiments. A 2-m-wide line source upslope of the monitoring trench was sprinkled continuously until a steady state flux was achieved at the trench (3–5 days). The flux into the bedrock was determined as the difference between the steady state sprinkling flux and the flux into the trench at the bottom of the hillslope. Under the assumption of unit head gradient, the saturated hydraulic conductivity of the bedrock was then calculated through dividing the bedrock flux by the area over which bedrock infiltration occurs (i.e. the product of the width of the line source and the distance between line source and trench).

This approach was repeated for three locations at each of 6, 9 and 14 m upslope of the trench. For the upslope sections, the loss was determined as the difference

between the volume applied, the volume captured in the trench and the measured loss in the section downslope. Losses and derived bedrock hydraulic conductivities were determined for nine 16 m<sup>2</sup> sections of the hillslope (see positions shown in Figure 1a). Despite high water application rates (0.291 s<sup>-1</sup> or approximately 44 mm h<sup>-1</sup>), no overland flow was observed.

To analyse the relationship between hydraulic conductivity and the bedrock topography that governs the direction of lateral subsurface flow, we calculated the flow accumulated area and topographic wetness index (TWI) of the bedrock topography. The cell size of the bedrock digital elevation model (DEM) was small compared with the size of the topographic depressions; hence, we used a D8 algorithm to calculate flow accumulation. The TWI was calculated with the following equation (Kirkby, 1975):

$$TWI = \ln(\alpha/\tan\beta) \quad (3)$$

where  $\alpha$  is the upslope area per unit contour length (m<sup>2</sup> m<sup>-1</sup>) and  $\beta$  is the local slope gradient (°). The unit contour length was 1 m in this study.

#### Model setup

We developed a distributed hydrological model to simulate the spatial distribution of GWR.

We assumed that all throughfall (the fraction of precipitation that is not intercepted by vegetation) infiltrated into the soil. The throughfall volume was calculated with an empirical formula (Equation (4)) determined by Tromp-van Meerveld and McDonnell (2006a) from storm events at PMRW (Cappellato and Peters, 1995).

$$T = 0.97P - 1.66 \quad (4)$$

where  $T$  is the throughfall depth of a rainstorm (mm) and  $P$  is the depth of the rainstorm (mm). For potential transpiration rate of the vegetation, we used the average daily rate of 2.6 mm day<sup>-1</sup> measured during the 2002 growing season. In the model simulations, the actual transpiration per timestep from each soil column was determined as the minimum of two volumes:

$$T_{ACT} = \min(T_{POT}, S_{ACT}) \quad (5)$$

where  $T_{ACT}$  is the actual volume of transpiration (m),  $T_{POT}$  is the potential volume of transpiration (m) and  $S_{ACT}$  is the actual volume of water stored in the soil column (m). We assumed an immediate and uniform distribution of moisture in the soil column. Where there was no soil present, water was immediately added to the SBI reservoir.

The soil was represented by a single column above each bedrock topography cell. We assumed unsaturated flow was a consequence of gravity drainage only (i.e. unit

gradient flow) (Equation (6)):

$$q_V = -K_{eff} \quad (6)$$

where  $q_V$  is the unsaturated flux (m day<sup>-1</sup>) and  $K_{eff}$  is the effective conductivity (m day<sup>-1</sup>). The effective hydraulic conductivity (Equation (7)) was calculated as a function of the saturated hydraulic conductivity and the relative conductivity:

$$K_{eff} = K_V K_r \quad (7)$$

where  $K_V$  is the saturated hydraulic conductivity of the soil in vertical direction (m day<sup>-1</sup>) and  $K_r$  is the relative conductivity (-), calculated with the van Genuchten–Mualem equation (van Genuchten, 1980):

$$K_r = \sqrt{\frac{\theta_a - \theta_r}{\theta_s - \theta_r}} \left( 1 - \left( 1 - \left( \frac{\theta_a - \theta_r}{\theta_s - \theta_r} \right)^{\frac{1}{m}} \right)^m \right)^2 \quad (8)$$

where  $\theta_a$  is the actual soil moisture content,  $\theta_s$  the saturated soil moisture content and  $\theta_r$  the residual soil moisture content. The  $m$  (-) parameter is related to the shape parameter  $n$  (-) from the van Genuchten water retention curve through the following:

$$m = 1 - 1/n \quad (9)$$

Groundwater recharge was determined as a direct loss from the SBI reservoir. If there was water present in this reservoir at any point of the hillslope, the recharge rate,  $q_{gwr}$  (m day<sup>-1</sup>) was determined as the minimum of two rates:

$$q_{gwr} = \min(q_V, K_{BR}) \quad (10)$$

where  $q_V$  is the drainage from the soil (m day<sup>-1</sup>) and  $K_{BR}$  (m day<sup>-1</sup>) is the saturated hydraulic conductivity of the bedrock. The storage capacity of the bedrock was assumed to be infinite.

When the recharge rate into the bedrock was too small to drain the SBI reservoir during the timestep, water was routed along the SBI topography. The routing algorithm takes into account changes in flow directions caused by filling and spilling of depressions in the microtopography (Appels *et al.*, 2011). We replaced the original instantaneous water transfer in the redistribution algorithm with a kinematic wave approximation of the Boussinesq equation over a sloping boundary (Equation (11), Rupp and Selker (2006)) to account for the spatial variability of horizontal hydraulic conductivity:

$$Q_L = K_L b h \frac{dH}{dx} \quad (11)$$

where  $Q_L$  is the lateral flux of water (m<sup>3</sup> day<sup>-1</sup>),  $K_L$  is the saturated hydraulic conductivity of the soil in lateral direction (m day<sup>-1</sup>),  $b$  is the width of flow (m),  $h$  is the height of the saturated layer (m) and  $dH/dx$  is the

hydraulic head gradient ( $\text{mm}^{-1}$ ), that is assumed to be equal to the gradient of the bedrock surface in the direction of flow. The flow direction along the SBI was determined for every timestep, based on the highest local gradient of the hydraulic head. The resulting flow was then calculated in a single direction (Equation (11)).

The height of the saturated zone was transient and assumed to be unrelated to the soil column height, implying the presence of a transient thin soil layer for saturated flow at the locations where the bedrock was exposed. At the domain boundary, water was allowed to drain freely from the seepage face without outflow resistance. The conceptualization of soil and saturated zone above the SBI is illustrated in Figure 2.

#### Generation of fields of hydraulic conductivity

Our model required three spatial distributions of hydraulic conductivity: vertical and lateral direction in the soil and vertical in the bedrock. Spatially variable fields of hydraulic conductivity were generated from the results of a geostatistical analysis of the conductivity measurements. The geostatistical analysis of the measurements was performed with the nlme and geoR packages of R statistical software (Diggle and Ribeiro, 2007; Pinheiro *et al.*, 2013). Based on the best-fitting models for the measurements, as presented in Table III, random fields were generated with the RandomFields package (Schlather *et al.*, 2014) of R statistical software (R Core Team, 2014). The random field generation was

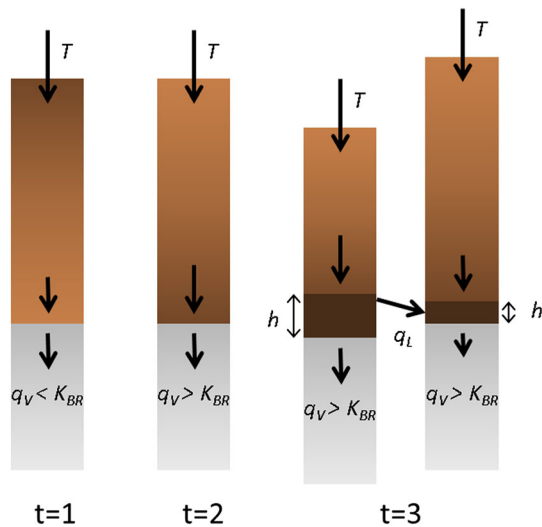


Figure 2. Illustration of the subsurface conceptualization at three subsequent timesteps during a rainstorm. At  $t = 1$ , the soil is still unsaturated and the vertical flux from the soil is smaller than the maximum  $K_{BR}$ . Because of the wetting of the soil column at  $t = 2$ , the vertical flux from the soil is now larger than the flux into the bedrock and a saturated layer starts to form at the soil-bedrock interface. At  $t = 3$ , water in the saturated layer moves laterally from one column to its neighbouring soil column

performed with the log10 transformed measurement values because of non-normally distributed values in the dataset (see Section on Spatial patterns of soil and bedrock saturated hydraulic conductivity).

The  $K_L$  dataset was large enough for a reliable estimate of the spatial distribution of the values, and the number of measurements of  $K_V$  and  $K_{BR}$  was smaller and measurements represented a smaller part of the hillslope.  $K_{BR}$  was measured at a larger spatial scale than the cell size of the generated spatial distributions of  $K_{BR}$ . However, we assumed that the variance of the measurements was equal to the variance of the smaller spatial scale. We recognize that the limited number of  $K_{BR}$  measurements means that the estimates of nugget and correlation length of the covariance model (Table III) are highly uncertain. However, the generated fields do not contain unreasonable values for  $K_{BR}$  given our knowledge of the site. With the assumption of this covariance model (Table III), we were able to explore the hydrological interactions between spatially variable fields of  $K_L$ ,  $K_V$  and  $K_{BR}$ . We do realize that these interactions are sensitive to the ratios of correlation lengths of the three types of conductivity fields. Investigating that sensitivity was beyond the scope of this paper.

#### Parameterization and simulation scheme

Model simulations were performed with 25 combinations of randomly generated hydraulic conductivity fields. We established with a jackknife resampling analysis that the standard deviation of the water balance components did not change when considering 20 simulations or more, suggesting that the results of our set of 25 simulations are not biased to a specific combination of hydraulic conductivity patterns.

The soil hydraulic parameters required for the calculation of the relative conductivity (Equation (8)) were uniformly distributed ( $\theta_s = 0.45$ ,  $\theta_r = 0.30$ ,  $n = 1.75$ ). These values were based on calibration results of previous modelling studies (Hopp and McDonnell, 2009; James *et al.*, 2010). The grid cell size of the domain was set at 0.25 m, such that the heterogeneity of the bedrock topography could be distinguished.

We performed three sets of simulations of increasing complexity to address the effects of the following: (1) spatial variability of hydraulic conductivity, (2) storm duration and (3) transient precipitation on GWR on the hillslope. Table I presents the parameterization scheme of the simulation sets.

The rainfall event of simulation set 1 has been described and modelled before by Burns *et al.* (2001), Freer *et al.* (2002), Hopp and McDonnell (2009), and James *et al.* (2010). The rainfall volume was corrected for throughfall (Equation (4)), but transpiration was neglected as this event occurred before the growing season.

The first combination of conductivity values in this first simulation set (Table II) was based on the average of the measured values of soil and bedrock hydraulic conductivity with a relatively small contrast between vertical hydraulic conductivity of the soil and bedrock (simulations a and d). For the second and third combination, the contrast between  $K_V$  and  $K_{BR}$  was increased by a factor of 10 (simulations b and e) and a factor of 100 (simulations c and f). Initial conditions and spin up period were the same as used by James *et al.* (2010).

The intensity and lag time used in simulation set 2 were the average storm intensity and the average lag time between storms at Panola, calculated from the 147 storm record (Tromp-van Meerveld and McDonnell, 2006a). In these simulations, transpiration was neglected, and the rainfall events were treated as effective throughfall events.

The precipitation series of simulation set 3 was corrected for throughfall (Equation (4)), and the potential transpiration rate was set at  $2.6 \text{ mm day}^{-1}$  during the growing season (1 May to 1 October). In the analysis of these simulations, event duration was defined as the length of the rainstorm and the following 24 dry hours.

## RESULTS

### *Spatial patterns of soil and bedrock saturated hydraulic conductivity*

The measured hydraulic conductivity values of the three zones showed a large variability (Figure 3 and Table III). The  $K_V$  profiles measured with the Guelph permeameter showed a general tendency of decreasing variability of hydraulic conductivity with depth. However, large values were found at 45 and 72 cm depth (Figure 3). These may be attributed to the presence of macropores or other vertical preferential flow paths in the soil as identified as important transport mechanisms

Table II. Saturated hydraulic conductivity values used in the simulations presented in Figure 5

Simulation	Spatially uniform	Spatially variable	Soil	Soil	Bedrock
			vertical ( $K_V$ ) ( $\text{cm h}^{-1}$ )	lateral ( $K_L$ ) ( $\text{cm h}^{-1}$ )	( $K_{BR}$ ) ( $\text{cm h}^{-1}$ )
a		d	2.5	67	0.83
b		e	2.5	67	0.083
c		f	25	67	0.083

Simulations a–c were parameterized with the mean values of the spatially variable fields of simulations d–f.

by Freer *et al.* (2002). We did not find a statistically significant relation between soil depth and saturated hydraulic conductivity, neither in the vertical nor in the lateral direction.

The ranges of the measured values of saturated hydraulic conductivity of the soil and bedrock overlapped. A Kolmogorov–Smirnov test showed that the lateral saturated hydraulic conductivity ( $K_L$ ) of the soil was significantly larger than the vertical saturated hydraulic conductivity of the soil ( $K_V$ ) and the bedrock ( $K_{BR}$ ), but there was no significant difference between the datasets of  $K_V$  and  $K_{BR}$  at a  $p$ -value of 0.10. The size of the  $K_L$  values could also have been affected by the local slope of the SBI, reflecting differences in hydraulic head instead of variability of  $K_L$ . An analysis of measured  $K_L$  values, grouped by soil depth, *versus* slopes determined from the bedrock DEM did not reveal a correlation between saturated hydraulic conductivity and local slope. In addition, Figure 4a and b shows no meaningful correlations of measured  $K_L$  values and flow accumulation or TWI based on the bedrock DEM.

Geostatistical analysis of the data showed that a lognormal distribution fitted the observed spatial clustering of hydraulic conductivity better than a normal

Table I. Overview of setup of the simulations

	Simulation scheme – effect of:		
	1. Uniform and spatial variability of hydraulic conductivity	2. Storm duration	3. Transient precipitation
$K_V, K_L, K_{BR}$	3 realizations of spatially variable K and 3 realizations of spatially uniform K. Values presented in Table II.	25 realizations of spatially variable K generated with geostatistics presented in Table III.	25 realizations of spatially variable K generated with geostatistics presented in Table III.
Forcing	A single long rainfall event that occurred on 6 and 7 March 1996, during which 87 mm of rain precipitated following a dry period of 7 days.	100 mm rain precipitated at a rate of $5 \text{ mm h}^{-1}$ in 1, 2, 5, 10 or 20 rainfall events. Each event is followed by a 4.5 day dry spell.	A full year of precipitation, measured in 1997.
Initial condition	$\theta_i = 0.375$	$\theta_i = 0.38$ and $\theta_i = 0.32$	$\theta_i = 0.38$

SPATIAL PATTERNS OF BEDROCK GROUNDWATER RECHARGE

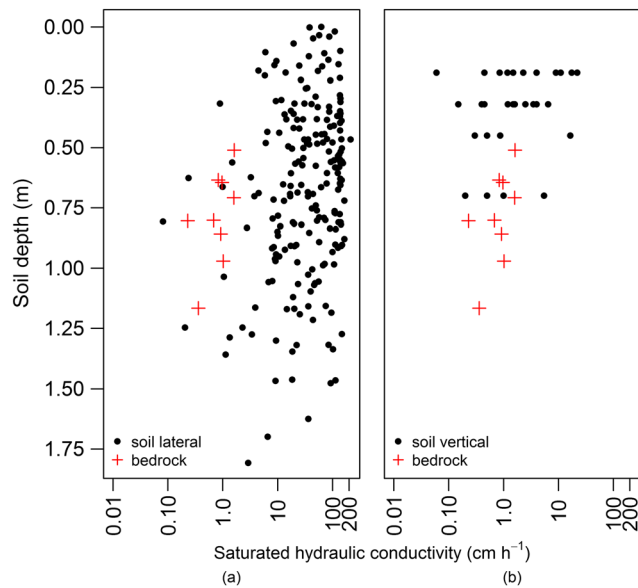


Figure 3. Measured values of saturated hydraulic conductivity plotted against soil depth: (a) conductivity of the soil in lateral direction and bedrock conductivity and (b) conductivity of the soil in vertical direction and bedrock conductivity. Note the logarithmic x-axis

Table III. Statistics of saturated hydraulic conductivity of the soil and bedrock

	Measured (log10 transformed values of $\text{cm h}^{-1}$ )			Fitted exponential (log10 transformed values of $\text{cm h}^{-1}$ )			
	Mean	Variance	Min–max range	Mean	Variance	Nugget	Correlation length (m)
Soil vertical ( $K_V$ )	-0.17	0.34	-1.2 to 1.3	-0.05	0.59	0.0	15.6
Soil lateral ( $K_L$ )	1.5	0.36	-1.1 to 2.3	1.5	0.38	0.26	20.6
Bedrock ( $K_{BR}$ )	-0.11	0.078	-0.64 to 0.21	-0.11	0.078	0.0	30.5

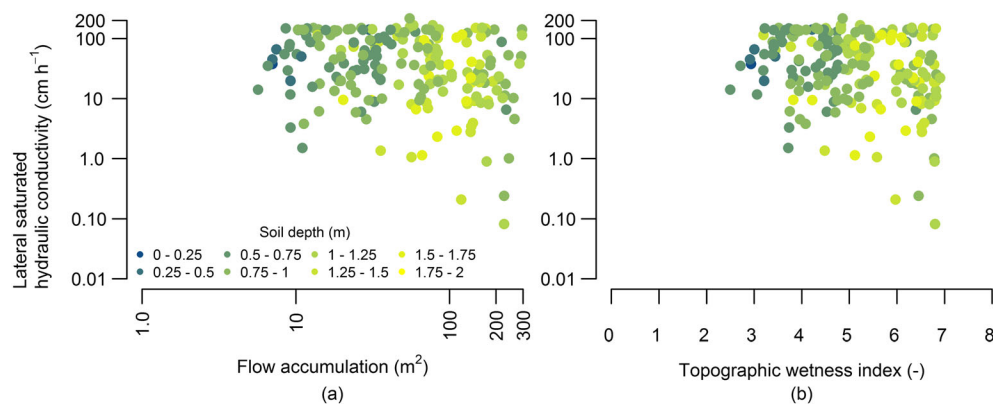


Figure 4. Lateral soil saturated hydraulic conductivity plotted versus (a) the flow accumulation area of the bedrock topography and (b) topographic wetness index (TWI) of the bedrock topography. For both flow accumulation area and TWI, the 80-percentile value of all points within 1 m radius of each well was used. The colour coding indicates average soil depths around the wells

distribution. An exponential covariance model provided the best fit to all three datasets (Table III). The coefficient of variation (CV) of measured hydraulic conductivity of both

$K_V$  and  $K_{BR}$  was larger than that of  $K_L$ . The correlation length of the fitted covariance models was shortest for the soil hydraulic conductivity in the vertical direction.

### Effects of uniform and spatially variable hydraulic conductivity

In the simulations with uniform parameters (Figure 5a–c), only soil depth and bedrock topography control the spatial pattern of GWR that results after a rainstorm. When the contrast between  $K_V$  and  $K_{BR}$  was small (Figure 5a),  $q_V$  from the soil exceeded  $K_{BR}$  only at locations with soil depths smaller than 0.05 m and lateral flow along the SBI did not extend further than 1 m before reinfiltration. Shallow soil zones were more saturated than deep soil zones, and therefore, higher amounts of GWR occurred in these zones during the course of the storm. In the uniform simulations with a larger contrast between  $K_V$  and  $K_{BR}$  (Figure 5b and c),  $q_V$  from the soil exceeded the  $K_{BR}$  early on in the rainstorm and as a result zones with shallow soils now generated lateral flow along the SBI. Zones of high flow accumulation and depression storage in the bedrock topography developed a larger transient saturated layer that provided high GWR in the drainage phase after the storm. Because of the formulation of the  $q_L$  in one direction and the lack of detailed topography of the bedrock, the lateral flowpaths along the SBI appear as ribbons of increased GWR in the final maps.

Although the cumulative bedrock GWR did not exceed the event precipitation at the hillslope scale, local values of GWR could be much higher as a result of lateral flow and slow recharge from the stagnating saturated layer after the storm: up to a factor three for the uniform conductivity fields and a factor five for the spatially variable conductivity fields.

In the simulations with spatially variable values of  $K_V$ ,  $K_L$  and  $K_{BR}$ , we found that firstly the rate at which water was delivered to the SBI was affected: Some deeper soil zones now received more GWR than others in the low-contrast simulation (Figure 5d). Secondly, the spatial distribution of  $K_L$  created a more varied pattern of lateral flow. So while the GWR ribbons were still visible in Figure 5e and f, the GWR pattern surrounding these hotspots of GWR was less smooth.

The low-contrast parameter set underestimated subsurface flow at the bottom of the domain most: no flow in the uniform scenario and only  $0.05 \text{ m}^3$  cumulative in the spatially variable version. The higher contrast parameter sets all generated significant subsurface flow with a first peak already occurring during the first rain period of the storm. This was an artefact of the model structure that just considered one soil layer and therefore simulated a fast movement of the infiltration front. The spatial distribution of  $K_V$  partly mitigated this artefact, because it caused a slight delay of the first runoff peak and a more prolonged drainage phase of the hydrographs after the storm (Figure 5e and f). Simulations c and f resulted in cumulative runoff volumes closest to the observed total runoff of  $13.5 \text{ m}^3$ , suggesting that this conductivity contrast approaches reality best.

### Effects of storm duration

Figure 5 showed a clear negative relationship between soil depth and GWR when hydraulic conductivities were uniformly distributed; the pattern became more varied with spatially variable fields of  $K$ . In Figure 6, the spatial variability of the GWR pattern is shown as a function of storm duration. The CV was determined for all cells that fell within the same soil depth range. The total amount of rain applied was the same in all the scenarios, although this volume was applied in a varying number of storms (Table I, simulation set 2). Consequently, the total amount of GWR was the same too. However, the fraction of total recharge during storms increased disproportionately with the size of an individual storm event from 7% in the 1-h storms to 78% in the 20-h storm. In accordance with this increase, the lines in each panel of Figure 6 display a trend of increasing variability with storm duration, even though there were considerable differences between the individual combinations of fields (a result of  $K_V$  variability). In shallower soil classes, the range of CV (i.e. the bandwidth of the lines in Figure 6) increased because of effects of  $K_{BR}$  variability: The vertical flux from the soil was larger than the flux into the bedrock. In the deeper soil classes, the range of CV increased more slowly because the soil did not reach similar levels of saturation. Increased CV could be attributed to run-on from shallower soil zones.

The extent of lateral flow can be illustrated by comparing the actual saturated area of the SBI with the area where saturation was generated because the flux from the soil was larger than  $K_{BR}$ . Figure 7 illustrates the increasing extent of run-on with increasing storm duration. The loops in the panels are hysteretic: The saturated area increases during the storm and then sustains saturation during the drainage phase both because percolation rates from wet shallow soil zones are still high and because drainage from the saturated layer continues after the storm. Longer storms resulted in a larger saturated SBI area and more deviation from the 1 : 1 line, indicating a larger travel distance of lateral flow. The differences between the loops of the individual combinations of  $K$  fields show that the exact size and position of the run-on affected areas depends on the particular realization of  $K_L$  and  $K_{BR}$  fields.

### Analysing the groundwater recharge pattern – annual precipitation dynamics

The spatial patterns of soil and bedrock conductivity affected mainly that annual cumulative subsurface runoff and storage change in the transient saturated layer at the SBI. This is illustrated in Table IV by the high coefficients of variation for these water balance components.

Figure 8 shows the empirical cumulative distribution function of GWR and cumulative rainfall as a function of

SPATIAL PATTERNS OF BEDROCK GROUNDWATER RECHARGE

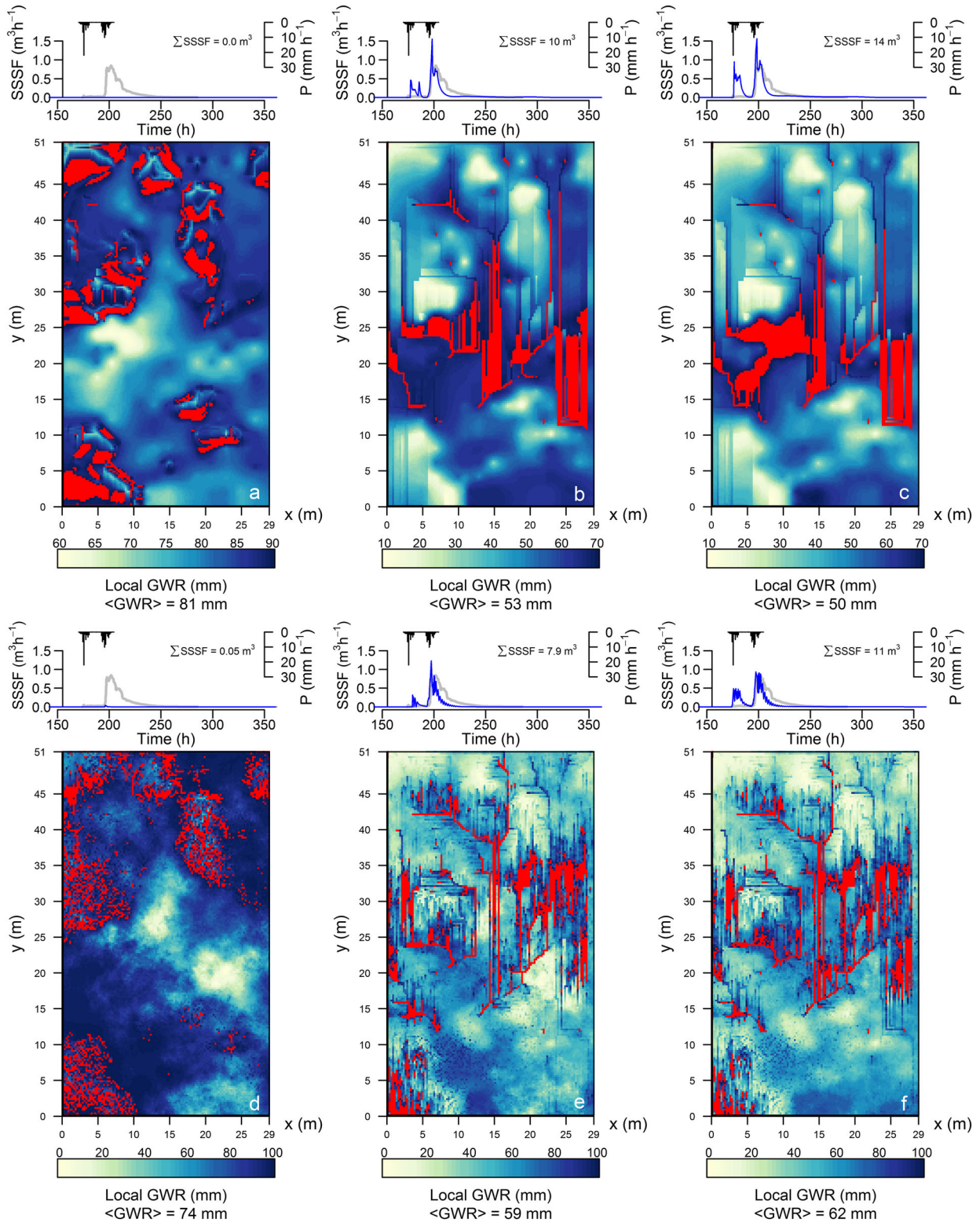


Figure 5. Hydrographs and maps of bedrock groundwater recharge after the 6–7 March 1996 rain storm. The grey line is the observed hydrograph in the trench, and the black line the input precipitation and the blue line the hydrograph of subsurface flow at the bottom of the model domain. The maps show cumulative bedrock groundwater recharge from the start of the rain storm until the end of the simulation (7 days) in every grid cell. The colour scales vary between the simulations. The red dots indicate locations with bedrock groundwater recharge higher than the 90-percentile value. The simulations of panels a–c were performed with spatially uniform  $K_V$ ,  $K_L$  and  $K_{BR}$  (values presented in Table II), and those of panels d–f with spatially variable fields of  $K_V$ ,  $K_L$  and  $K_{BR}$  (values presented in Table II)

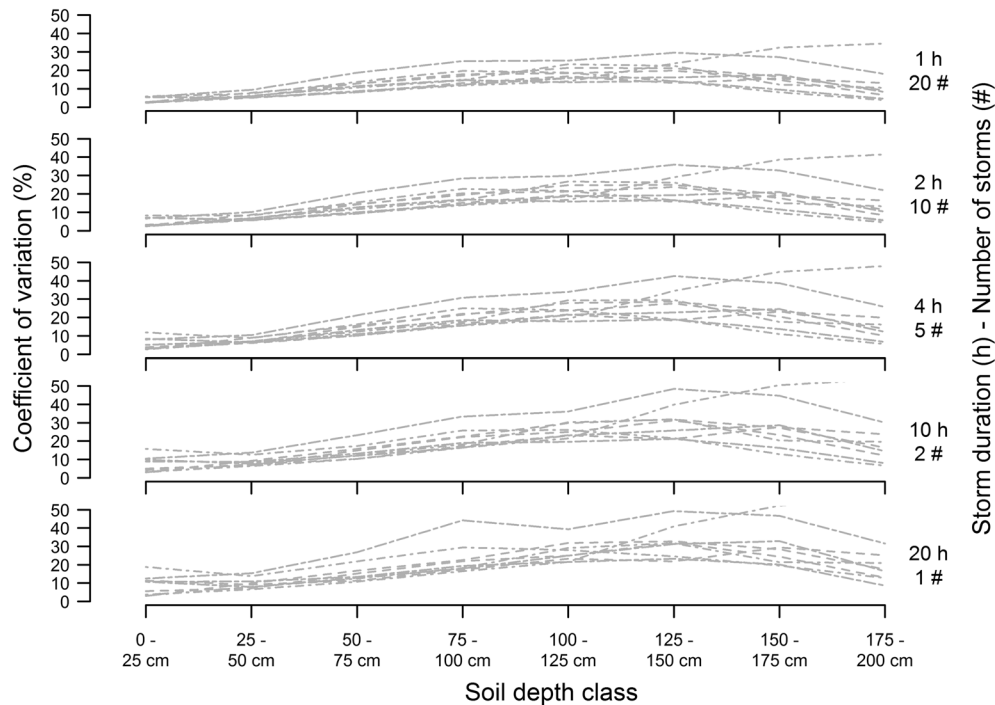


Figure 6. Coefficient of variation of groundwater recharge (%) determined in eight classes of soil depth. Each panel contains the results of a precipitation scenario presented in Table I (forcing of simulation set 2). A precipitation scenario consists of 100 mm rain applied at a rate of  $5 \text{ mm h}^{-1}$ , but in a varying number of storms within the simulation (with storm duration increasing while the number of storms in the simulation decreases). Each grey line represents one of 25 simulations with a random combination of  $K_V$ ,  $K_L$  and  $K_{BR}$ . For clarity, only 12 out of 25 simulations have been plotted

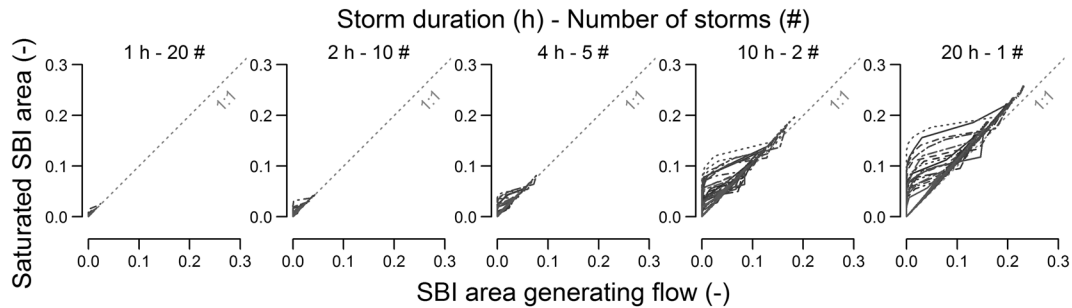


Figure 7. Saturated areal fraction of soil-bedrock interface (SBI) plotted against the areal fraction of SBI where the percolation rate is larger than  $K_{BR}$  and subsurface lateral flow is generated. Each line represents one of 25 simulations with a random combination of  $K_V$ ,  $K_L$  and  $K_{BR}$

event throughfall. Our simulations showed that 25% of annual GWR occurred during events with 9.7 mm throughfall or less, 50% of annual GWR during events with throughfall of 37 mm or less and 75% of annual GWR during events with throughfall of 84 mm or less (Figure 8). A total of 40% of annual GWR occurred during events that exceeded the Tromp-van Meerveld and McDonnell (2006a) precipitation threshold for subsurface flow of 52 mm throughfall.

Groundwater recharge under saturated areas accounted for 40% of the annual total GWR.

Maps of cumulative GWR during various periods of the simulation and of different realizations of  $K$  fields are shown in Figure 9. These maps show that GWR hotspots

(in red) changed with storm magnitude. In a lag period (Figure 9a), the zones with deep soil received the largest amounts of GWR, whereas in an event period with the same average amount of GWR (Figure 9b), more recharge occurred in zones with shallow soil. Events needed to be of a considerable size to have increased GWR occur along lines of higher flow accumulation (Figure 9d). The relative contribution of GWR hotspots to the total volume varied per event between 12% and 90%, depending on the extent of lateral flow. On a yearly timescale (Figure 10), the hotspots received 30% of the bedrock GWR.

Three zones could be distinguished when the yearly cumulative GWR at each point of the hillslope was plotted as a function of the duration of saturation at the

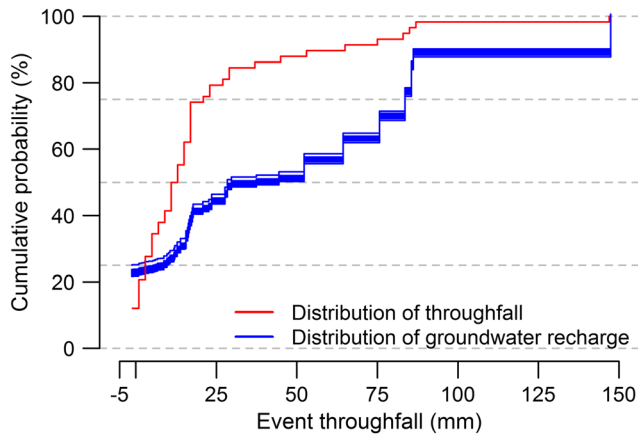


Figure 8. Cumulative distribution of annual bedrock groundwater recharge and throughfall as a function of event throughfall amount for all 25 simulations. A negative event throughfall indicates net transpiration in the current event definition

between rain depth ( $\Sigma P$ ) and soil water storage capacity ( $V_{soil}$ ) determines the size of the vertical flux of water through the soil. Secondly, the ratio between this vertical flux ( $q_V$ ) and the flux into the bedrock ( $q_{gwr}$ ) determines the level of saturation at the SBI. Thirdly, the ratio between the lateral flux ( $q_L$ ) from saturated areas at the SBI and the flux into the bedrock ( $q_{gwr}$ ) determines the run-on distances along the SBI. In these three phases, a structural hillslope characteristic influences the dynamic control. When the first and second ratios are small, the spatial pattern will reflect the spatial distribution of soil depth. Conversely, when widespread SBI saturation occurs, run-on distances are large and increased GWR will occur within zones of high flow accumulation and depression storage in the bedrock topography (SBI<sub>topo</sub>). In the transition phase, during which increased  $q_V$  and limited SBI saturation are combined, the  $K_L$  pattern on the hillslope controls run-on distances and locations of

Table IV. Water balance components of full year simulation mean (standard deviation) of the 25 random realization combinations

	Throughfall	Transpiration	Groundwater recharge	Runoff	Storage change unsaturated soil	Storage change saturated layer
Yearly mean and standard deviation (m <sup>3</sup> )	1800 (0)	419 (0.7)	1337 (7)	47 (7)	-7.2 (1)	4.2 (3)
Percentage of yearly throughfall (%)	100	23	74	2.6	-0.4	0.2

SBI (Figure 10): (1) a zone without a strong correlation between duration of saturation and amount of GWR, (2) a zone where long durations of saturation corresponded to high yearly GWR and (3) a zone displaying the same correlation but at a steeper slope.

## DISCUSSION

### *A perceptual model of the spatial hierarchy of groundwater recharge at the hillslope scale*

Our simulations suggest that the relative importance of each of the structural and dynamic controls on GWR into bedrock at the hillslope scale varies with rainstorm size and the duration of dry periods between events. The structural aspects of the hillslope include its bedrock topography, soil depth, soil hydraulic properties – characteristics that are assumed to be constant on the recharge timescale. The dynamic aspects include the rate at which water is delivered to, and the extent to which lateral flow is present at the SBI – characteristics that are transient on the recharge timescale.

We conceptualize that the dynamic aspects drive the hierarchy of controls shown in Figure 11. Firstly, the ratio

increased bedrock GWR.

Our results show that the spatial variability of soil depth trumps the spatial variability of  $K_V$  as a factor controlling the spatial pattern of GWR. This is because in our simulations the spatial variability of the delivery rate is mainly determined by the soil moisture content. Shallow soil zones not only deliver more water to the SBI than deeper zones and at a higher rate. This is because they reach a state of higher saturation than their deeper soil counterparts during average rainstorms. The spatial variability of  $K_V$  plays a smaller role, affecting the variation around the GWR–soil depth relationship.

The presence of fractures or other bedrock permeability enhancements is a structural aspect for increased bedrock GWR potential (as opposed to an average value of bedrock permeability as estimated by Tromp-van Meerveld *et al.*, 2007). Fractures will act as hot spots for GWR, because of their large potential loss rate. Although our model does not explicitly account for fracture flow, the randomly generated fields of  $K_{BR}$  contained points with values large enough to be considered as fractures. Our results show that the combined vertical and lateral flux is not always large enough for the *actual* loss rate to equal the *potential* loss

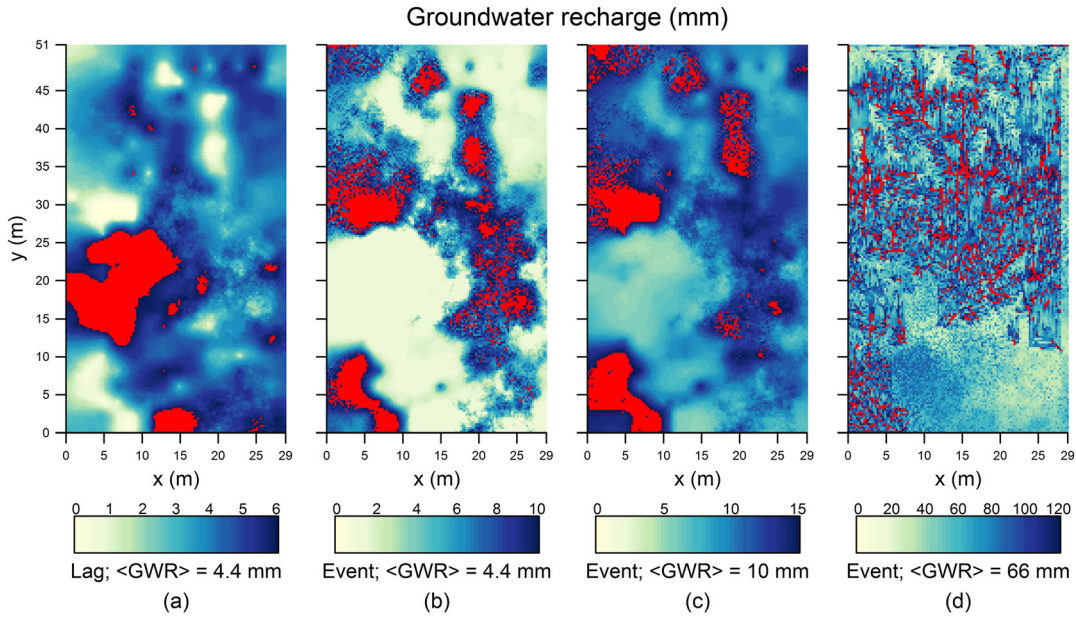


Figure 9. Maps of cumulative groundwater recharge of one lag between rain events and three events of increasing size (a–d). Every colour scale is cut off at the 90-percentile value of groundwater recharge during the specific period. The locations in red are the locations where groundwater recharge is larger than the 90-percentile value. An event was defined as rainstorm duration plus the following 24 dry hours. A lag was defined as a dry period beyond those 24 h until the start of the subsequent rainstorm

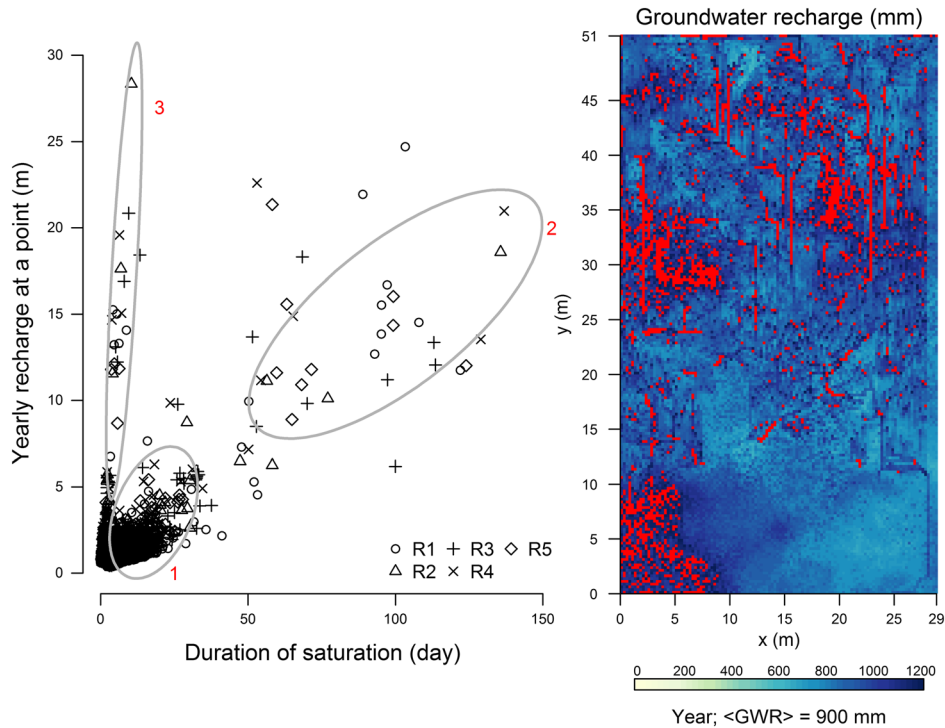


Figure 10. Cumulative groundwater recharge at a point as a function of the duration of saturation for five random realizations (left, realizations indicated with different symbols). Map of yearly cumulative groundwater recharge (right). The colour scale was cut off at the 90-percentile value of groundwater recharge and the locations with higher groundwater recharge coloured red

rate. Instead, increased bedrock GWR will also occur at locations with smaller  $K_{BR}$  but with accompanying prolonged saturation at the SBI. In general, lateral flow

ceases within 24h after rainfall events and the saturated layer is drained by vertical recharge into the bedrock. Recharge from this saturated layer occurs faster than

Structural characteristics enhance dynamic controls locally

Dynamic characteristics drive hierarchy of controls

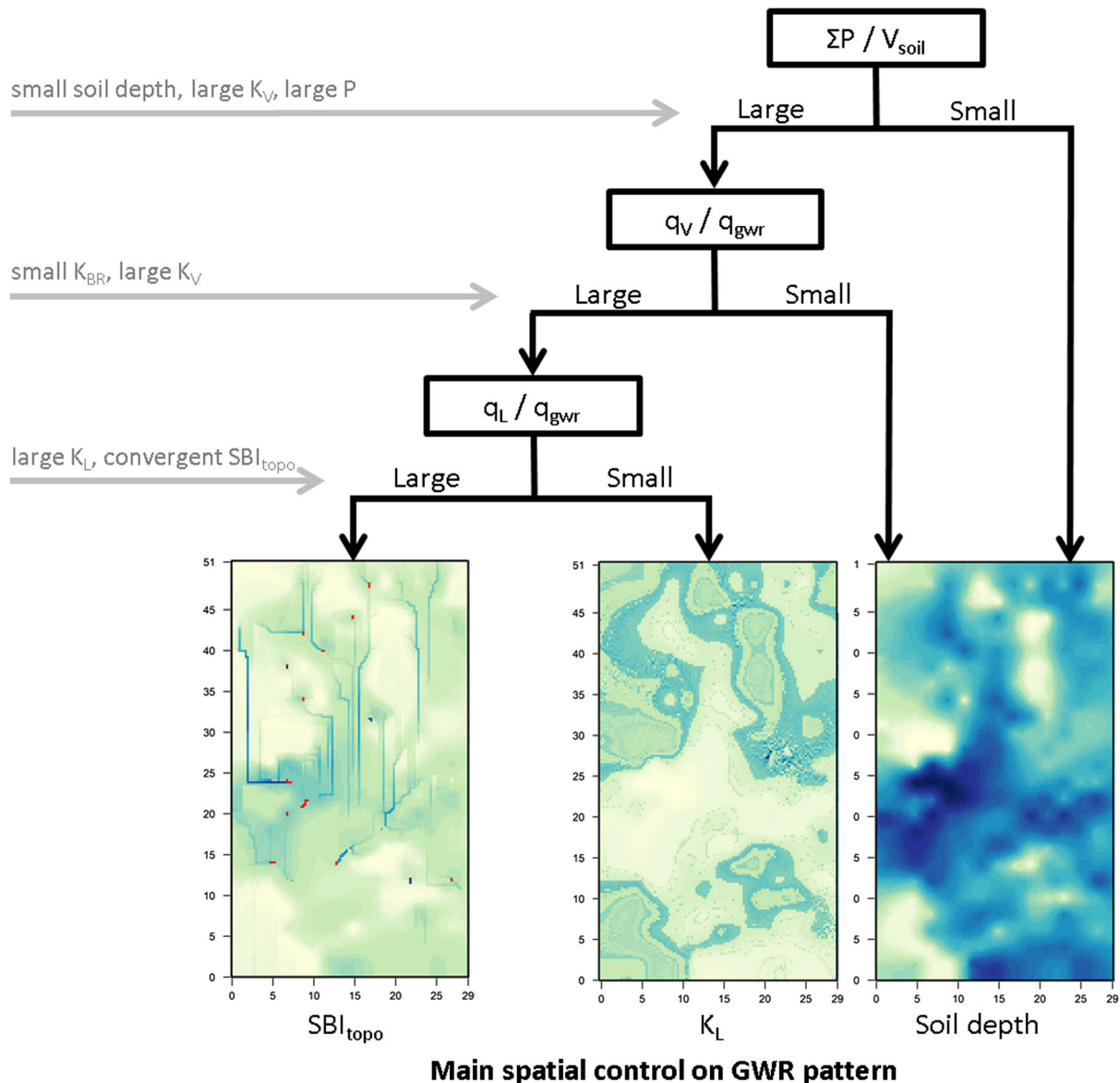


Figure 11. Conceptual model of generation of a spatial pattern of groundwater recharge at the Panola hillslope. The structural characteristics that reinforce the effect of a dynamic control are indicated in grey on the left side of the figure

drainage from the soil and is the main reason why the 'fraction of recharge occurring during rain storms' increases nonlinearly with storm size.

The storm throughfall amount determines the extent over which saturation at, and lateral flow along, the SBI occurs. Lateral flow occurred during virtually all rainfall events in our simulations, but it did not always make it farther downslope than cells directly neighbouring the locations where it was generated.

In our simulations, high flow accumulation zones were the main control on GWR patterns during rainstorms larger

than 50 mm throughfall or smaller storms on a very wet (>60% saturation) soil. This 50 mm is fairly consistent with the 52 mm throughfall threshold for subsurface flow at Panola as found by Tromp-van Meerveld and McDonnell (2006b) and in more recent rules-based modelling of Janzen and McDonnell (2015). In the hydrological year that we investigated, 10% of the annual throughfall occurs in events larger than that threshold. These events provide 40% of the simulated annual GWR. On an annual basis, 23% of simulated GWR occurs between storms, during which soil depth is the main control on the GWR pattern.

The remaining 33% of GWR occurs in ‘transition phase’ rainstorms, with relatively short run-on distances. In this transition phase, sections of the hillslope are in different stages of the hierarchy in Figure 11 during the same event.

Consistent with Hopp and McDonnell (2009) and Harman and Sivapalan (2009), the average soil depth, bedrock permeability, soil hydraulic conductivity and lower boundary conditions determine the hillslope integrated water balance. However, individual spatial distributions of these hillslope characteristics strongly determine the spatial pattern of bedrock GWR hotspots. When defined as locations with GWR greater than the 90-percentile value, 30% of annual GWR occurs in hotspots (i.e. 10% of the hillslope area receives 30% of the hillslope recharge). However, the contribution and the position of hotspots depends on the timescale that is chosen to analyse GWR.

Our perceptual model of bedrock GWR shows that the dynamic aspects driving the spatial pattern of bedrock GWR, i.e. rainstorm size in proportion to soil water storage capacity, are key factors in the occurrence and positioning of recharge hotspots. Our perceptual model of GWR occurring at short distances downslope of the original point of infiltration of throughfall fits well into the interflow framework proposed by Jackson *et al.* (2014). It accounts for saturated zones developing in a fragmented fashion along the hillslope, converging along lines of flow accumulation when storms are large. This model is consistent with the fill-and-spill of bedrock topography in the sense that in order to generate subsurface stormflow at the lower boundary of the hillslope, the fill zones need to be fully saturated and connected. However, these zones do not map one-to-one to hotspot positions of GWR, because of the heterogeneity that is created by short distance run-on during events below the threshold.

#### *On groundwater recharge and measurement scale*

We caution that the results presented in this paper are simulation results. The overlap of simulated patches of transient saturation at the SBI with increased GWR is promising, but we cannot evaluate our model with measured values of bedrock GWR at the site – a notoriously difficult measurement to make (Shand *et al.*, 2005; Heppner *et al.*, 2007; Gleeson *et al.*, 2009; Salve *et al.*, 2012). That said, experimental studies at other hillslope sites have reported both the distinctive slow, widespread recharge during dry periods *versus* fast, localized recharge in wet periods (Anderson *et al.*, 1997; Gleeson *et al.*, 2009) and large differences in magnitude of response in individual wells to events (Salve *et al.*, 2012).

In this study, we have shown how spatially variable distributions of conductivity play a role in creating a

recharge flux that is highly variable in space and time. We combined two sets of point-scale measurements (Guelph permeameter and well-based falling head measurements) with more integrated measurements (sprinkling experiment) to generate spatial distributions of conductivity on our hillslope. We worked from the premise that these experiments provided a range of values of soil and bedrock conductivity and a first quantitative measure of their spatial correlation but not a set of exact values at each point of the hillslope.

The sprinkling experiments at various sections of the hillslope above the trench showed a large range of  $K_{BR}$  variability (consistent with the sprinkling experiment performed by Tromp-van Meerveld *et al.* (2007)), even though the section areas were still rather large and individual fractures were not mapped or instrumented. In order to estimate the actual locations of increased bedrock recharge (e.g. everything higher than the 90-percentile value as per Figure 10), quantifying the local extent of lateral flow along the SBI is an important step. Our work suggests that because of the higher frequency of small rainstorms and the resulting occurrence of lateral flow over short distances at the site, the spatial distribution of  $K_L$  is as important as that of  $K_{BR}$ . The well-based falling head experiment, as simplistic as it was, provided some insights into that distribution. The experimental method had some drawbacks: (1) the direction of flow was not well defined (saturation around the wells most likely occurred as a “bulb” of wetting) and (2) it was a combined measurement of soil and bedrock permeability so that neither could be individually resolved. The latter is not an issue if the contrast between soil and bedrock permeability is high. Notwithstanding these issues, one of the interesting measurement results was that these ranges of conductivity overlap. This may imply that local conductivity contrasts are smaller than generally acknowledged at the site until now (compare the high average contrast calculated by Tromp-van Meerveld *et al.*, 2007). It may further imply that some of the well-based falling head measurements measured the conductivity of the bedrock and not that of the soil. Since the soil consists of colluvium originating from upslope parent material, it is perhaps not surprising that the saturated hydraulic conductivity of soil and bedrock are not spatially correlated. However, given the occurrence of subsurface flow on the site, we expected that  $K_L$  above the SBI would be related to topographic characteristics of the bedrock that govern lateral flow. Where lateral flow accumulates, more weathering could result in eroded soil pipes or, conversely, clogging due to flushing and accumulation of fine materials. Hence, we expected a correlation of  $K_L$  with flow accumulation or TWI. The lack of such a correlation (Figure 4) illustrates the need of separate spatial surveys of conductivity at other sites

instead of using bedrock topography or soil depth as a proxy for the distribution of  $K_L$ .

A logical follow up would be a detailed survey of distributions of hydraulic conductivity at a site such as Rivendell (Salve *et al.*, 2012; Kim *et al.*, 2014) to see if these can be used to explain the lack of uniformly rising and falling perched groundwater table at the site. It is intuitive to focus measurement campaigns on large events that feature subsurface runoff at the toe of a hillslope, but for improving our understanding of spatial variability of GWR more emphasis should be put on measuring flow distances during smaller events.

#### *On the value of a simple modelling approach*

The results of this study show that the location of hotspots of bedrock GWR is determined largely by the spatial distribution of lateral soil hydraulic conductivity, bedrock hydraulic conductivity and the extent of lateral flow that is generated on the hillslope during a multi-storm time series.

The first weakness of our modelling approach is that we did not simulate flow through the bedrock matrix and fractures. The unlimited unit gradient flux into the bedrock likely overestimates recharge under unsaturated drainage conditions and underestimates such fluxes during periods of transient saturation at the SBI. Also, we did not simulate return flow from upslope fractures into the soil further downslope and thus ignore feedbacks between bedrock and soil as for instance observed by Montgomery *et al.* (1997) and Shand *et al.* (2007). Secondly, we restricted lateral flow to the SBI, where a more sophisticated physical model could simulate perched groundwater flow at any depth in the soil profile. The rationale for the assumption of restricted lateral flow is found in previous field and modelling studies at the site that have shown that saturated flow mainly occurs at this interface.

The lack of bedrock flow simulation is more difficult to defend as we do not have data to support our modelling choices. The shallow bedrock geology of the hillslope likely contains connected fractures parallel to the land surface because it is constructed from granite blocks (Tromp-van Meerveld *et al.*, 2007). Connected fractures in the bedrock may produce return flow from the bedrock into the hillslope, but there is no experimental evidence confirming or negating this. Previous modelling studies of the Panola hillslope by Hopp and McDonnell (2009) and James *et al.* (2010) contained hydrologically active bedrock but did not consider fracture flow either.

Incorporating both the spatial variability of saturated hydraulic conductivity of soil and bedrock, and bedrock topography on a hillslope while running a model that deals with matrix and fracture flow remains a computa-

tional challenge. Modelling studies of similar hydrogeological systems with more sophisticated numerical tools (e.g. HydroGeoSphere by Gleeson *et al.*, 2009) are therefore necessarily restricted to a simpler description of their modelling domain. In a recent study with a 3D Richards' solver by Liang and Uchida (2014), soil depth and TWI were found to be first-order controls on transient saturation at the SBI in a steep catchment with a high intensity rainstorm. As shown in this study, this is an extreme scenario; on gentle hillslopes and during shorter rain events local flow heterogeneities are likely more important controls. Alternatively, instead of using more powerful Darcy–Richards solvers for this type of problem that feature non-Darcian flow in both soil and bedrock, different conceptual approaches to fast recharge such as the one proposed by Mirus and Nimmo (2013) may be a successful way forward.

## CONCLUSIONS

We examined the spatio-temporal distribution of bedrock GWR at the hillslope scale at the well-studied Panola experimental hillslope. We used new measurements of spatially variable soil and bedrock hydraulic conductivity and a multi-event precipitation series to perform simulations of GWR with a new, simple, spatially distributed model.

We found that the major part of simulated GWR during a hydrological year occurred under unsaturated drainage. Soil depth was a main control on amounts and rates through available storage capacity and controlling the size of vertical flux. During rain storms transient saturation occurred at the SBI and lateral flow started to affect GWR patterns. There were two aspects to that. Firstly, hillslope SBI locations that received more lateral flow and had increased saturation at the end of a storm received more GWR. Secondly, increased lateral flow transported water to locations where the bedrock permeability was higher.

We have shown that under the rainfall regime found at Panola and the specific distribution of soil and bedrock hydraulic properties, hillslope-wide SBI saturation only occurred during extreme rainfall events. While these contributed a large amount of water, the main controls on an annual scale were therefore not just soil depth and bedrock topography, i.e. the factors that control fill-and-spill areas in the subsurface. Instead, hydraulic conductivity, both that of bedrock and the 'lateral' soil, determined the activation and extent of lateral flow along the SBI.

The results of this study highlight the importance of 3D modelling and simulation of multi-storm time series when investigating GWR distributions. Point-scale modelling by definition underestimates the variability of the process and cannot account for variation in location and timing of

increased bedrock GWR as does modelling at the watershed scale. This is in accordance with results of subsurface stormflow studies. We propose that in order to improve our understanding of the spatio-temporal dynamics of GWR at the hillslope scale, we go back to subsurface runoff hillslopes and try to quantify the characterizing ratios between delivery and loss rate and rain storm size and extent of lateral flow.

## REFERENCES

- Allison G, Gee G, Tyler S. 1994. Vadose-zone techniques for estimating groundwater recharge in arid and semiarid regions. *Soil Science Society of America Journal* **58**(1): 6–14.
- Anderson SP, Dietrich WE, Montgomery DR, Torres R, Conrad ME, Loague K. 1997. Subsurface flow paths in a steep, unchanneled catchment. *Water Resources Research* **33**(12): 2637–2653.
- Appels WM, Bogaart PW, van der Zee SEATM. 2011. Influence of spatial variations of microtopography and infiltration on surface runoff and field scale hydrological connectivity. *Advances in Water Resources* **34**(2): 303–313.
- Asano Y, Uchida T, Ohte N. 2002. Residence times and flow paths of water in steep unchanneled catchments, Tanakami, Japan. *Journal of Hydrology* **261**(1–4): 173–192.
- Bachmair S, Weiler M. 2011. New dimensions of hillslope hydrology. In *Forest Hydrology and Biogeochemistry. Synthesis of Past Research and Future Directions*, Levina DF, et al. (eds). Springer: Netherlands; 455–481.
- Barron OV, Crosbie RS, Dawes WR, Charles SP, Pickett T, Donn MJ. 2012. Climatic controls on diffuse groundwater recharge across Australia. *Hydrology and Earth System Science* **16**(12): 4557–4570.
- Bouwer H, Rice R. 1976. Slug test for determining hydraulic conductivity of unconfined aquifers with completely or partially penetrating wells. *Water Resources Research* **12**(3): 423–428.
- Burns DA, McDonnell JJ, Hooper RP, Peters NE, Freer JE, Kendall C, Beven K. 2001. Quantifying contributions to storm runoff through end-member mixing analysis and hydrologic measurements at the Panola Mountain research watershed (Georgia, USA). *Hydrological Processes* **15**(10): 1903–1924.
- Buttle JM, McDonald DJ. 2002. Coupled vertical and lateral preferential flow on a forested slope. *Water Resources Research* **38**(5): 1060.
- Cappellato R, Peters N. 1995. Dry deposition and canopy leaching rates in deciduous and coniferous forests of the Georgia piedmont – an assessment of a regression-model. *Journal of Hydrology* **169**(1–4): 131–150.
- De Vries J, Simmers I. 2002. Groundwater recharge: an overview of processes and challenges. *Hydrogeology Journal* **10**(1): 5–17. DOI:10.1007/s10040-001-0171-7.
- Diggle PJ, Ribeiro PJ. 2007. *Model-based Geostatistics*. Springer: New York.
- Ebel BA, Loague K. 2008. Rapid simulated hydrologic response within the variably saturated near surface. *Hydrological Processes* **22**(3): 464–471.
- Flint LE, Flint AL, Stolp BJ, Danskin WR. 2012. A basin-scale approach for assessing water resources in a semiarid environment: San Diego region, California and Mexico. *Hydrology and Earth System Sciences* **16**(10): 3817–3833.
- Freer J, McDonnell JJ, Brammer D, Beven K, Hooper R, Burns D. 1997. Topographic controls on subsurface stormflow at the hillslope scale for two hydrologically distinct catchments. *Hydrological Processes* **11**(9): 1347–1352.
- Freer J, McDonnell JJ, Beven KJ, Peters NE, Burns DA, Hooper RP, Aulenbach B, Kendall C. 2002. The role of bedrock topography on subsurface storm flow. *Water Resources Research* **38**(12): 5–1–5–16.
- Gabrielli C, McDonnell JJ, Jarvis T. 2012. The role of bedrock groundwater in rainfall-runoff response at hillslope and catchment scales. *Journal of Hydrology* **450–451**: 117–133.
- Gleeson T, Novakowski K, Kyser TK. 2009. Extremely rapid and localized recharge to a fractured rock aquifer. *Journal of Hydrology* **376**(3–4): 496–509.
- Graham C, Barnard H, van Verseveld W, McDonnell JJ. 2010. Estimating the deep seepage component of the hillslope and catchment water balance within a measurement uncertainty framework. *Hydrological Processes*. DOI:10.1002/hyp.7788.
- Harman C, Sivapalan M. 2009. Effects of hydraulic conductivity variability on hillslope-scale shallow subsurface flow response and storage-discharge relations. *Water Resources Research* **45**. DOI:10.1029/2008WR007228.
- Heppner CS, Nimmo JR, Folmar GJ, Gburek WJ, Risser DW. 2007. Multiple-methods investigation of recharge at a humid-region fractured rock site, Pennsylvania, USA. *Hydrogeology Journal* **15**(5): 915–927.
- Hopp L, McDonnell JJ. 2009. Connectivity at the hillslope scale: identifying interactions between storm size, bedrock permeability, slope angle and soil depth. *Journal of Hydrology* **376**: 378–391. DOI:10.1016/j.jhydrol.2009.07.047.
- Jackson CR, Bitew M, Du E. 2014. When interflow also percolates: downslope travel distances and hillslope process zones. *Hydrological Processes* **28**(7): 3195–3200.
- James A, McDonnell JJ, Tromp van Meerveld I, Peters NE. 2010. Gypsies in the palace: experimentalist's view on the use of 3-D physics based simulation of hillslope hydrological response. *Hydrological Processes* **24**: 3878–3893. DOI:10.1002/hyp.7819.
- Janzen D, McDonnell JJ. 2015. A stochastic approach to modelling and understanding hillslope runoff connectivity dynamics. *Ecological Modelling* **298**: 64–74.
- Kim H, Bishop JKB, Dietrich WE, Fung IY. 2014. Process dominance shift in solute chemistry as revealed by long-term high-frequency water chemistry observations of groundwater flowing through weathered argillite underlying a steep forested hillslope. *Geochimica et Cosmochimica Acta* **140**: 1–19.
- Kirkby M. 1975. Hydrograph modelling strategies. In *Processes in Physical and Human Geography*, Peel R, et al. (eds). Heinemann: London; 69–90.
- Kosugi K, Katsura S, Katsuyama M, Mizuyama T. 2006. Water flow processes in weathered granitic bedrock and their effects on runoff generation in a small headwater catchment. *Water Resources Research* **42**(2). DOI:10.1029/2005WR004275.
- Liang WL, Uchida T. 2014. Effects of topography and soil depth on saturated-zone dynamics in steep hillslopes explored using the three-dimensional Richards' equation. *Journal of Hydrology* **510**: 124–136.
- Mair A, Hagedorn B, Tillery S, El-Kadi AI, Westenbroek S, Ha K, Koh G-W. 2013. Temporal and spatial variability of groundwater recharge on Jeju Island, Korea. *Journal of Hydrology* **501**: 213–226.
- McDonnell JJ. 2013. Are all runoff processes the same? *Hydrological Processes* **27**(26): 4103–4111. DOI:10.1002/hyp.10076.
- Mirus BB, Nimmo JR. 2013. Balancing practicality and hydrologic realism: a parsimonious approach for simulating rapid groundwater recharge via unsaturated-zone preferential flow. *Water Resources Research* **49**(3): 1458–1465.
- Montgomery DR, Dietrich WE, Torres R, Anderson SP, Heffner JT, Loague K. 1997. Hydrologic response of a steep, unchanneled valley to natural and applied rainfall. *Water Resources Research* **33**(1): 91–109.
- Montgomery DR, Dietrich WE. 2002. Runoff generation in a steep, soil-mantled landscape. *Water Resources Research* **38**(9): 1168.
- Pangle LA, Gregg JW, McDonnell JJ. 2014. Rainfall seasonality and an ecohydrological feedback offset the potential impact of climate warming on evapotranspiration and recharge. *Water Resources Research* **50**(2): 1308–1321. DOI:10.1002/2012WR013253.
- Peters DL, Buttle JM, Taylor CH, Lazerte BD. 1995. Runoff production in a forested, shallow soil, Canadian Shield basin. *Water Resources Research* **31**(5): 1291–1304.
- Pinheiro J, Bates D, DebRoy S, Sarkar D, R Development Core Team. 2013. nlme: linear and nonlinear mixed effects models.
- R Core Team. 2014. *R: a language and environment for statistical computing*. R Foundation for Statistical Computing: Vienna, Austria.

- Rupp DE, Selker JS. 2006. On the use of the Boussinesq equation for interpreting recession hydrographs from sloping aquifers. *Water Resources Research* **42**(12). DOI:10.1029/2006WR005080.
- Salve R, Rempe DM, Dietrich WE. 2012. Rain, rock moisture dynamics, and the rapid response of perched groundwater in weathered, fractured argillite underlying a steep hillslope. *Water Resources Research* **48**. DOI:10.1029/2012WR012583.
- Scanlon BR, Healy RW, Cook PG. 2002. Choosing appropriate techniques for quantifying groundwater recharge. *Hydrogeology Journal* **10**(1): 18–39.
- Schlather M, Malinowski A, Oesting M, Boecker D, Strokorb K, Engelke S, Martini J, Menck P, Gross S, Burmeister K, Manitz J, Singleton R, Pfaff B, R Core Team. 2014. RandomFields: simulation and analysis of random fields.
- Shand P, Haria AH, Neal C, Griffiths KJ, Goody DC, Dixon AJ, Hill T, Buckley DK, Cunningham JE. 2005. Hydrochemical heterogeneity in an upland catchment: further characterisation of the spatial, temporal and depth variations in soils, streams and groundwaters of the Plynlimon forested catchment, Wales. *Hydrology and Earth System Sciences* **9**(6): 621–644.
- Shand P, Darbyshire DPF, Goody D, Haria AH. 2007. <sup>87</sup>Str/<sup>86</sup>Sr as an indicator of flowpaths and weathering rates in the Plynlimon experimental catchments, Wales, U.K. *Chemical Geology* **236**(3–4): 247–265.
- Torres RWE, Dietrich DR, Montgomery SP, Anderson KL. 1998. Unsaturated zone processes and the hydrologic response of a steep, unchanneled catchment. *Water Resources Research* **34**(8): 1865–1879. DOI:10.1029/98WR01140.
- Troch PA, Berne A, Bogaart P, Harman C, Hilberts AGJ, Lyon SW, Paniconi C, Pauwels VRN, Rupp DE, Selker JS, Teuling AJ, Uijlenhoet R, Verhoest NEC. 2013. The importance of hydraulic groundwater theory in catchment hydrology: the legacy of Wilfried Brutsaert and Jean-Yves Parlange. *Water Resources Research* **49**(9): 5099–5116.
- Tromp-van Meerveld I, McDonnell JJ. 2006a. Threshold relations in subsurface stormflow 1: a 147 storm analysis of the Panola hillslope trench. *Water Resources Research* **42**. DOI:10.1029/2004WR003778.
- Tromp-van Meerveld HJ, McDonnell JJ. 2006b. Threshold relations in subsurface stormflow 2: the fill and spill hypothesis: an explanation for observed threshold behavior in subsurface stormflow. *Water Resources Research* **42**. DOI:10.1029/2004WR003800.
- Tromp-van Meerveld HJ, Peters NE, McDonnell JJ. 2007. Effect of bedrock permeability on subsurface stormflow and the water balance of a trenched hillslope at the Panola Mountain Research Watershed, Georgia, USA. *Hydrologic Processes* **21**: 750–769.
- Tromp-van Meerveld HJ, McDonnell JJ. 2009. On the use of multi-frequency electromagnetic induction for the determination of temporal and spatial patterns of hillslope soil moisture. *Journal of Hydrology* **368**(1): 56–67.
- van Genuchten MT. 1980. A closed-form equation for predicting the hydraulic conductivity of unsaturated soils. *Soil Science Society of America Journal* **44**: 892–898.
- White AF, Bullen TD, Schulz MS, Blum AE, Huntington TG, Peters NE. 2001. Differential rates of feldspar weathering in granitic regoliths. *Geochimica et Cosmochimica Acta* **65**(6): 847–869.
- White AF, Blum AE, Schulz MS, Huntington TG, Peters NE, Stonestrom DA. 2002. Chemical weathering of the Panola Granite: solute and regolith elemental fluxes and the weathering range of biotite. In *Water–Rock Interactions, Ore Deposits, and Environmental Geochemistry: A Tribute to David A. Crerar*. Hellmann R, Wood SA (eds). The Geochemical Society: St Louis, MO, USA; **7**: 37–59.
- Wilson CJ, Dietrich WE. 1987. The contribution of bedrock groundwater flow to storm runoff and high pore pressure development in hollows. *IAHS Publication* **165**: 49–59.